Biochimica et Biophysica Acta 1848 (2015) 1175–1182

Contents lists available at ScienceDirect

Biochimica et Biophysica Acta

journal homepage: www.elsevier.com/locate/bbamem

Hydroxytyrosol and tyrosol esters partitioning into, location within, and effect on DOPC liposome bilayer behavior☆

Kervin O. Evans *, Joseph A. Laszlo, David L. Compton

Renewable Products Technology Research Unit, National Center of Agricultural Utilization Research Center, Agricultural Research Service, U.S. Department of Agriculture, 1815 N. University Street, Peoria, IL 61604, USA

ARTICLE INFO

Article history:
Received 8 October 2014
Received in revised form 2 February 2015
Accepted 6 February 2015
Available online 14 February 2015

Keywords:
Hydroxytyrosol
Tyrosol
Bilayer depth
Partitioning

ABSTRACT

The phenols hydroxytyrosol and tyrosol made abundantly available through olive oil processing were enzymatically transesterified into effective lipophilic antioxidants with cuphea oil. The hydroxytyrosyl and tyrosyl esters made from cuphea oil were assessed for their ability to partition into, locate within and effect the bilayer behavior of 1,2-dioloeoylphosphatidylcholine liposomes and compared to their counterparts made from decanoic acid. Partitioning into liposomes was on the same scale for both hydroxytyrosyl derivatives and both tyrosyl derivatives. All were found to locate nearly at the same depth within the bilayer. Each was found to affect bilayer behavior in a distinct manner.

Published by Elsevier B.V.

1. Introduction

Liposomes are nanoscaled bubbles that separate an internal solution from an extravesicular one by a lipid bilayer where the hydrophilic head group of the lipids forms the outside of the bilayer and the hydrophobic chains form the inside of the bilayer [1]. Exploited for their ability to encapsulate hydrophobic and hydrophilic material, liposomes have been used in food industry to encapsulate bioactive materials such as vitamins (antioxidants), peptides and antimicrobial molecules [2]. It has been demonstrated that liposomes have the ability to provide protection and enhancement to encapsulated material [3].

The antioxidant properties of tyrosol (2-(4-hydroxyphenyl)ethanol) and hydroxytyrosol (2-(3,4-dihydroxyphenyl)ethanol) (Fig. 1a), natural phenols obtained from olive biomass, make both of them highly desirable for use as preservatives in food and health applications [4,5]. Each can prevent undesired lipid oxidation at the cellular level based on their basic antioxidant activities. Lipophilic modifications through esterification of the primary alcohol group [6] have been made to both tyrosol and hydroxytyrosol to enhance their bioavailability. Modification with fatty acids of different lengths has proven not to diminish antioxidant capabilities, which follows the "polar paradox hypothesis" that indicates that the effectiveness of antioxidants in polar systems improves for more hydrophobic analogs [7]. However, "cut-off limits" to the "polar paradox hypothesis" have been demonstrated for rosmarinic acid at C_8 esters [8], chlorogenic acid at C_{12} [9], and hydroxytyrosol at C_{10} [10], above which efficacy declines. Based on the demonstrated maximized antioxidant ability of hydroxytyrosol lipophilic derivatives at C_{10} [10] and tyrosol at C_5–C_{16} [11], we previously synthesized hydroxytyrosol and tyrosol C_{10} esters from cuphea oil [12]. That work demonstrated not only that it was possible to efficiently synthesize hydroxytyrosyl and tyrosyl lipid esters of optimal chain length (C_{10}) using a natural and readily renewable oil, but their antioxidant properties within liposomes were comparable to the parent molecules (hydroxytyrosol and tyrosol) and their C_{10} esters synthesized from decanoic acid. Some basic questions, however, about the behavior of these hydroxytyrosol and tyrosol ester derivatives within liposomes were not answered. Those questions concerned partitioning ability, location within the bilayer and the ability to alter bilayer behavior in stability and perturbation (fusion and/or rupture and phase transition), as these attributes will influence their effectiveness in biological membranes

Abbreviations: HTyr, hydroxytyrosol; Tyr, tyrosol; DOPC, 1,2-dioleoyl-*sn*-glycero-3-phosphocholine; 1,2-dioleoyl-*sn*-glycero-3-phospho(tempo)choline, TEMPO-PC; 1-palmitoyl-2-stearoyl-(5-doxyl)-*sn*-glycero-3-phosphocholine, 5DOXYL-PC; 1-palmitoyl-2-stearoyl-(12-doxyl)-*sn*-glycero-3-phosphocholine, 12DOXYL-PC; HEPES, (4-(2-hydroxyethyl)-1-piperazineethanesulfonic acid; MPL, multilamellar phospholipid liposomes; Tyr-C_{10}, tyrosol decanoate; HTyr-C_{10}, hydroxytyrosol decanoate; HTyr-cupheate, hydroxytyrosol decanoate made from cuphea oil; Tyr-cupheate, tyrosol decanoate made from cuphea oil

☆ Mention of trade names or commercial products in this publication is solely for the purpose of providing specific information and does not imply recommendation or endorsement by the United States Department of Agriculture (USDA). USDA is an equal opportunity provider and employer.

* Corresponding author.
E-mail address: Kervin.Evans@ars.usda.gov (K.O. Evans).

http://dx.doi.org/10.1016/j.bbamem.2015.02.002
0005-2736/Published by Elsevier B.V.

and applications in food lipid matrices. The current work addresses these questions using fluorescence methods to measure partitioning into and location within 1,2-dioleoylphosphatidylcholine (DOPC; Fig. 1b) bilayers, a suitable liposome system for studying antioxidant incorporation [13,14]. This work also used quartz crystal microbalance with dissipation monitoring to determine ability to change bilayer behavior.

2. Experimental section

2.1. Materials

The following items were purchased as listed: tyrosol (2-(4-hydroxyphenyl)ethanol) (Tyr), (4-(2-hydroxyethyl)-1-piperazine-ethanesulfonic acid (HEPES), sodium chloride, solvents (HPLC grade; used without further purification), and decanoic acid were all from Sigma-Aldrich Co; hydroxytyrosol (2-(3,4-dihydroxyphenyl)ethanol) (HTyr) was from TCI America (Portland, OR); 1,2-dioleoyl-*sn*-glycero-3-phosphocholine (DOPC), 1,2-dioleoyl-*sn*-glycero-3-phospho(tempo)choline (TEMPO-PC), 1-palmitoyl-2-stearoyl-(5-doxyl)-*sn*-glycero-3-phosphocholine (5DOXYL-PC), and 1-palmitoyl-2-stearoyl-(12-doxyl)-*sn*-glycero-3-phosphocholine (12DOXYL-PC) were all from Avanti Polar Lipids (Alabaster, AL); cuphea oil (refined, bleached and deodorized from *Cuphea viscosissima* × *C. lanceolata* germplasm line PSR 23), as previously prepared [15].

2.2. Large liposomes

Liposomes were prepared as previously described [12]. Briefly, lipids in their solvents were mixed to the appropriate ratio in an amber vial and dried to a thin film under a gentle argon stream. HTyr and Tyr derivatives were added to lipids at 5-mol% of total lipid concentration. The dried lipids were rehydrated in the appropriate buffer and mixed periodically to form multilamellar phospholipid liposomes (MPLs). The MPLs were put through five freeze–thaw cycles and then extruded through two stacked 100-nm filters inside a LiposoFast extruder (Avestin, Ottawa, ON, Canada) to form extruded unilamellar liposomes (EULs). Liposomes were used immediately.

2.3. Partitioning into liposomes

Fluorescence was used to measure partitioning into phospholipid liposomes based on the Tyr and HTyr moieties' fluorescent signal that increases in a hydrophobic environment versus an aqueous one [16]. HTyr and Tyr esters were added to vials to a final concentration of 40 μM. Liposomes containing DOPC only were made as described above and diluted to the appropriate concentrations. Measurements were done using a Fluorolog 3–21 steady-state fluorometer (Jobin Yvon, Edison, NJ) equipped with a double-grating emission monochromator. The partition coefficient K_P was calculated by fitting the fluorescence intensities at a fixed wavelength to the following equation:

$$I(L) = I_o + I_{max}\frac{K_P * L}{W + K_P * L}, \quad (1)$$

where I_o was the initial fluorescence without EULs present; I_{max} was the maximal fluorescence increase upon full partitioning; L was the lipid molar concentration; W was water's molar concentration; and K_P was the molar fraction partition coefficient. Measurements were repeated three to six times.

2.4. Liposomal bilayer depth

The depth a molecule resides within the phospholipid bilayer was determined using parallax analysis. Parallax analysis is based on the ability to quench the fluorescence of the molecule of interest with phospholipids containing spin-labeling at various depths [17]. HTyr and Tyr derivatives have fluorescence intensities each that are collisionally quenchable by nitroxide-labeled lipids. The nitroxide spin-labeled phospholipids were TEMPO-PC, 5DOXYL-PC and 12DOXYL-PC (Fig. 1b) which each had the nitroxide quencher located in the headgroup region, at the C_5-position, and farther down the acyl chain at the C_{12}-position, respectively. Liposomes were made as described earlier containing 15-mole% of a spin-labeled phospholipid and 5-mole% of ester. The buffer contained 10 mM HEPES, 100 mM NaCl at pH 7.4.

The depth of fluorescent molecule within a bilayer was determined from the difference in quenching by the nitroxide-labeled using the following calculation [17,18]:

$$z_{cf} = L_{c1} + \left[-\ln(F_1/F_2)/\pi C - L_{21}^2\right]/2L_{21}; \quad (2)$$

where z_{cf} was the calculated distance the fluorophores were from the center of the membrane, F_1 was the normalized (with respect to liposomes containing only HTyr or Tyr derivatives and no spin-labeled phospholipids) emission fluorescence intensity in the presence of TEMPO-PC the "shallow" quencher, F_2 was the normalized fluorescence intensity in the presence of 5DOXYL-PC or 12DOXYL-PC (the "deep" quencher), L_{cl} was the distance between TEMPO-PC and the center of the bilayer, C was the concentration of quenchers per area (mole fraction of nitroxide-labeled lipids/area of lipid), and L_{21} was the difference in depth between quenchers. 70.1 $Å^2$ per molecule was the area assumed to be occupied by the phosphatidylcholine lipids [19]; 19.5 Å, 12.2 Å, and 5.9 Å were the distances from the bilayer center assumed for the TEMPO-PC, 5DOXYL-PC, and 12DOXYL-PC, respectively [20]. Data reported is the average of triple replicates.

2.5. Quartz crystal microbalance with dissipation (QCMD)

The QCMD technique provides information about adsorbed material based on the fact that a resonating quartz crystal will exhibit frequency shifts as mass binds to the surface [21]. The mass of any thin, rigid film adsorbed onto the surface can be described by the Sauerbrey equation [21]:

$$\Delta m = -\left(\frac{C}{n}\right)\Delta F, \quad (3)$$

where C is the sensitivity constant for quartz (17.7 ng/cm^2/Hz) at the fundamental frequency, n is the overtone number (1, 3, 5, 7, etc.), and ΔF is the frequency shift. The change in mass (Δm) includes all matter (trapped and adsorbed) coupled to the surface.

Liposome adsorption onto silicon oxide sensors was monitored using a QCMD-E4 system (Q-Sense, Biolin Scientific, Stockholm, Sweden). Frequencies (the fundamental and 6 overtones) were recorded during adsorption at 23 ± 0.1 °C. Buffer was injected at 75 μl/min across the sensors using a peristaltic pump (Ismatec IPC-N 4). Following establishment of a stable signal from the buffer injection, liposomes at 100 μM were injected across the sensors. Buffer was once again injected across the sensors after liposome adsorption or supported bilayer formation concluded. Measurements were repeated at least twice.

3. Results and discussion

HTyr and Tyr are phytochemicals with known fluorescence properties [22]. Their fluorescence emissions showed an increase in intensity and a spectral shift in organic solvents versus aqueous solutions (data not shown). This increase in fluorescence signal and spectral shift which occurred when HTyr and Tyr existed within a hydrophobic, less polar environment versus a hydrophilic, more polar one was an indication that water quenched the fluorescence, likely through hydrogen bonding [23]. This further suggested that partitioning of each

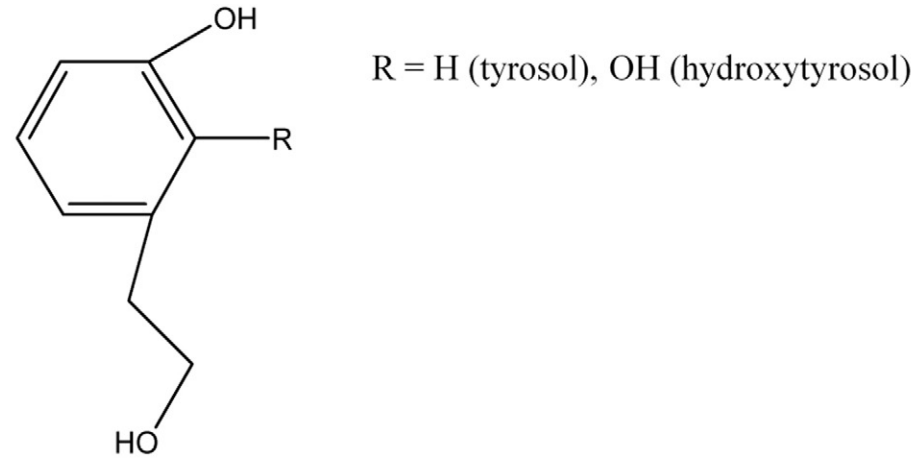

(a)

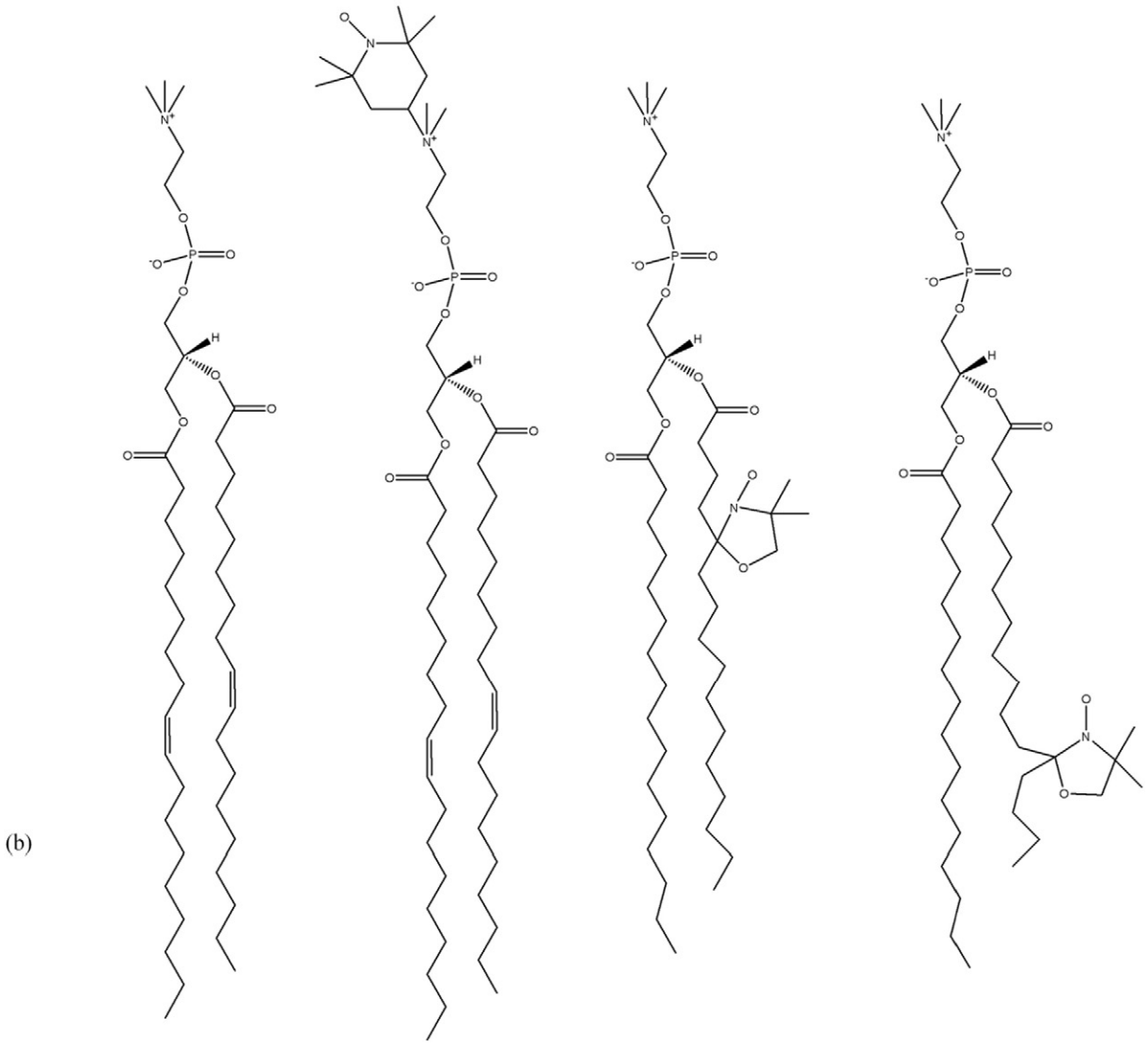

(b)

Fig. 1. Molecular representation of (a) HTyr, Tyr and (b) DOPC, TEMPO-PC, 5-DOXYL-PC, and 12-DOXYL-PC (left to right; not to scale).

phytochemical in liposomes can be monitored via fluorescence [16]. The affinity of the HTyr and Tyr derivatives synthesized from decanoic acid (herein referred to as HTyr-C_{10} and Tyr-C_{10}) and cuphea oil (HTyr-cupheate and Tyr-cupheate) was examined by titrating each derivative with DOPC liposomes. Fig. 2 shows the relative fluorescence intensity (ratio of fluorescence intensities for each derivative at increasing

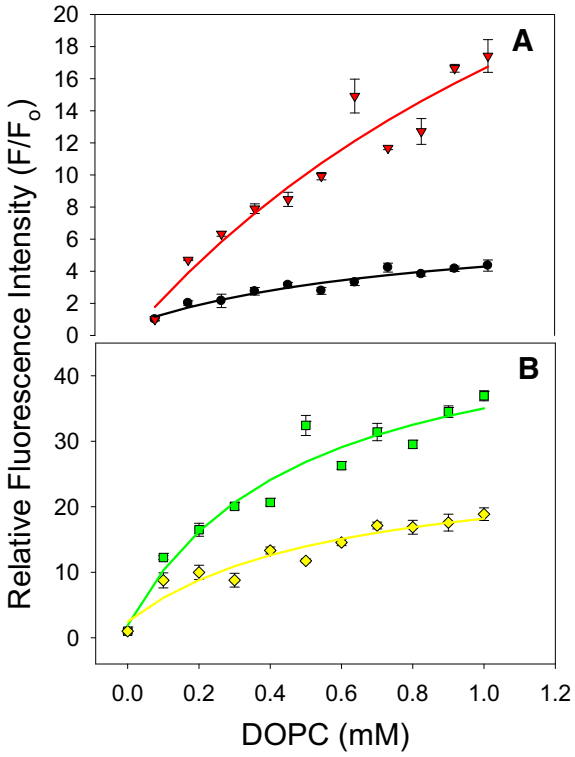

Fig. 2. Tyr (A) and HTyr (B) derivatives' relative fluorescence in 10 mM HEPES, 100 mM NaCl, pH 7.5 buffer as a function of DOPC liposomes. Relative fluorescence (I/I_o) was normalized in reference to the C_{10} derivatives with no liposomes present (I_o). The black filled circles (●) represent Tyr-C_{10}, the red-filled triangles (▲) represent Tyr-cupheate, the green-filled squares (■) represent HTyr-C_{10}, and the yellow-filled diamonds (♦) represent HTyr-cupheate. Data displayed is the average of three to six replicates.

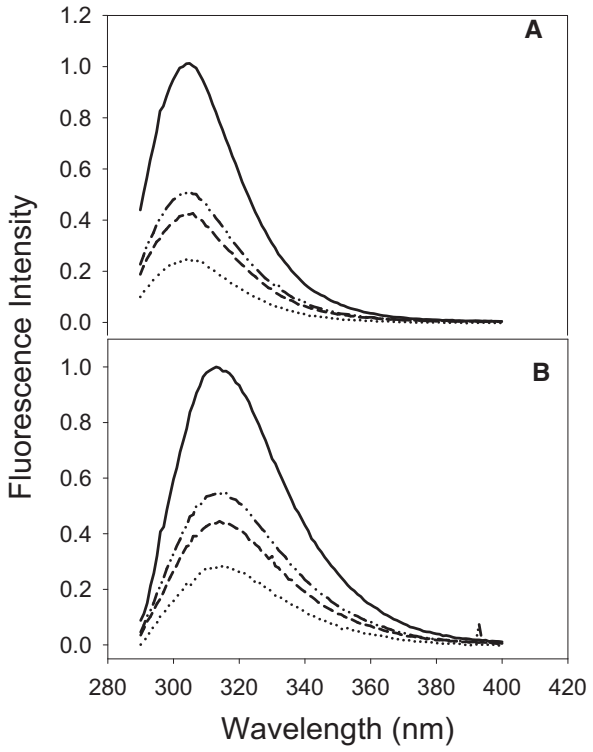

Fig. 3. Representative normalized fluorescence of Tyr-C_{10} (A) and HTyr-C_{10} (B) with and without spin-labeled lipids. Normalization was done with respect to the peak wavelength of each derivative incorporated into DOPC liposomes with no quencher present. The solid line represents the spectrum of the derivative without quencher present; the dotted line is the derivative with the TEMPO-PC quencher present; the dash/double dotted line is the 5-DOXYL-PC quencher; the dash line is the 12-DOXYL-PC quencher. Spectra were measured three times.

liposome concentration to that of derivatives with no liposomes—F/F_0) increase of each derivative (Tyr derivatives in Fig. 2a; HTyr derivatives in Fig. 2b) as they partition into DOPC liposomes. There was a 4- to 37-fold increase in the fluorescence signal of all derivatives, indicating a greater affinity for lipid membrane (DOPC) over water. Most likely the fluorescence increase was due to reduction of hydrogen bonding between the derivatives' phenol hydroxyl(s) group and water as the derivatives partitioned into the liposomes. The fitting curve (solid line) to the fluorescence increase in Fig. 2 resulted in slightly different partitioning values (Table 1) for the Tyr-C_{10} and Tyr-cupheate and nearly the same for HTyr-C_{10} and HTyr-cupheate. This was interpreted that both respective decanoic acid and cuphea oil derivatives of Tyr (HTyr) had similar affinity for lipid membranes. Surprisingly, the HTyr derivatives partitioned more readily than the Tyr derivatives (more specifically, each HTry derivative partitioned more readily than its Tyr counterpart), perhaps because the dual phenyl hydroxyl groups created a more amphiphilic molecule that more favorably partitioned across the interface of the bilayer region.

The parallax method allows the determination of a fluorescent molecule of interest's location (depth) within the bilayer through the quenching efficiency of spin-labeled probes [17]. Fig. 3 depicts the fluorescence spectra of the Tyr (Fig. 3A) and HTyr (Fig. 3B) derivatives within DOPC liposomes quenched by spin-labeled phospholipids. The all spin-labeled phospholipids showed the ability to quench the Tyr and HTyr moiety of each derivative with the TEMPO-PC spin-labeled lipid having the greatest quenching effect. Quenching displayed by each spin-labeled lipid indicates that there were subpopulations of each derivative residing at lower depths within the bilayer. Therefore, calculation of depth within the bilayer will express an overall average distance of all populations, which was ~20 Å for HTyr-cupheate and Tyr-cupheate, ~21 Å for HTyr-C_{10}, and ~22 Å for Tyr-C_{10} (Table 2) from the bilayer center. This placed all the moieties well within the aqueous interface of the bilayer. The fact that the Tyr and HTyr moieties of the derivatives existed within the same region of a bilayer indicates that their antioxidant differences previously demonstrated within liposomes [12] were likely due less to their location within the bilayer and more likely due to the two hydroxyl groups found in HTyr derivatives versus only one in Tyr derivatives. It should be noted that maximum emission wavelengths for Tyr-C_{10} and HTyr-C_{10} within liposomes (306 and 313 nm, respectively) are similar to the maximum emission wavelength for the esters below their CMC in water (303 nm and 313 nm, respectively). This wavelength maximum difference was

Table 1
Log P partitioning coefficient as determined from titration Tyr or HTyr derivatives with DOPC liposomes.

C_{10} derivative	Measured Log P
Tyr C_{10}	4.76
Tyr cupheate	4.43
HTyr C_{10}	5.05
HTyr cupheate	4.98

Table 2
Calculated distance from the bilayer center of Tyr and HTyr moieties in each derivative.

C_{10} derivative	Distance from bilayer center (Å)
Tyr decanoate	21.5 ± 0.3
Tyr cupheate	20.3 ± 0.4
HTyr decanote	20.5 ± 0.2
HTyr cupheate	20.3 ± 5.0

most probably caused by the difference in hydroxyl groups but does not rule out any possible effects due the respective moieties residing at slightly different regions which could provide different exposures to water and the polar environment, resulting in different effects on the spectra.

Incorporation of lipids, peptides, nanoparticles, and polymers has been demonstrated to affect bilayer behavior in phase transition [24, 25], shape and structure [26], fusion in solution [27], and perturbation and stability against fusion and rupture during surface adsorption [25]. Changes in perturbation and stability against fusion and rupture during surface adsorption were detectable using QCMD. Here, exploration of any effect that Tyr and HTyr derivatives have on perturbation and stability bilayer behavior was conducted using QCMD. The QCMD frequency and dissipation profiles for DOPC liposomes adsorbed onto silica surfaces exhibited typical frequency shift that maximized before increasing and reaching a plateau near −25 Hz. This was consistent with liposomal adsorption until a critical surface coverage occurred [28, 29] and with liposomes rupturing to expel water just prior to the formation of a stable supported bilayer (Fig. 4A, solid line). Liposomes containing 5-mole% HTyr-C_{10} also induced a negative frequency shift that maximized, followed by an increase to a plateau. This too was consistent with liposomes adsorbed to a critical concentration on

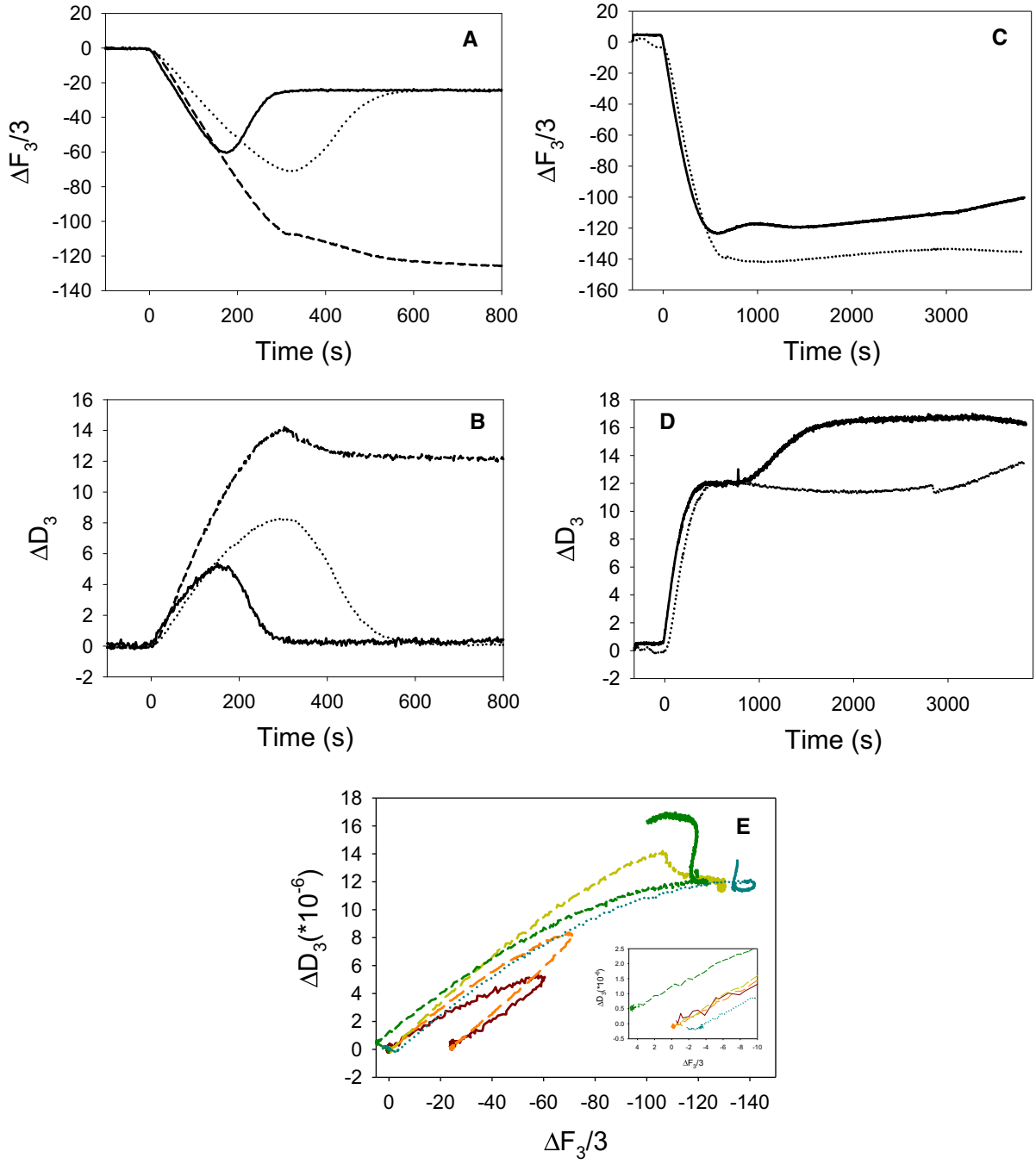

Fig. 4. QCMD response during the adsorption onto silica of DOPC liposomes incorporating HTyr and Tyr derivatives at 5-mole%. (A) and (B) are the frequency and dissipative responses (respectively) for DOPC (solid line), DOPC/HTyr-C10 (dotted line), and DOPC/Tyr-C10 (dashed line); (C) and (D) represent DOPC/HTyr-cupheate (solid line) and DOPC/Tyr-cupheate (dotted line); (E) ΔD vs. ΔF plots for DOPC containing all derivatives (DOPC—solid red line; DOPC/HTyr-C10—dashed orange line; DOPC/Tyr-C10—dashed yellow line; DOPC/HTyr-cupheate—dashed green line; DOPC/Tyr-cupheate—dotted blue line; insert displays the initial slopes of the plots—shown and calculated where adsorption began). Measurements were repeated at least twice.

silica before rupturing to expel their aqueous contents to form a supported bilayer at the same resting frequency and dissipation shifts as DOPC (Fig. 4A and B, dotted line). The notable difference between DOPC and DOPC/HTyr-C_{10} liposome adsorption was DOPC/HTyr-C_{10} liposomes required a longer time and slightly more liposomes to achieve critical surface coverage; these liposomes also required a longer time to expel their aqueous contents. The source of the longer rupture process of DOPC/HTyr-C_{10} versus DOPC liposomes may have several explanations. First, there is the possibility that the size of DOPC/HTyr-C_{10} was the source. DOPC/HTyr-C_{10} were 111 ± 0.5 nm in diameter versus 109 ± 0.3 nm of DOPC and larger liposomes have been shown to alter the activation energy for rupture on silica [30–32]. Secondly, HTry-C_{10} contains saturated C_{10} which may have raised the phase transition temperature in local areas within liposomes, resulting in an overall reduced fluidity and slowed rupture kinetics [33]. Reduced fluidity may also have resulted if the HTyr moiety increased packing within the aqueous interface of the bilayer as demonstrated by lutein in egg phosphatidylcholine [2].

The presence of 5-mole% Tyr-C_{10}, on the other hand, resulted in a greater negative frequency shift on the same time frame (~300 s) displayed by HTyr-C_{10} liposomes to reach critical surface coverage. The frequency shift then continued in a negative trend before stabilizing after nearly 800 s into the measurement. This indicates that the presence of Tyr-C10 reduced the interliposomal stress necessary for liposomes to rupture and form a supported bilayer; instead, liposomes adsorbed intact (Fig. 4A and B, dashed line). During the adsorption of DOPC/Tyr-C_{10} liposomes, approximately 86% of the liposomes adsorbed onto the surface and it required another ~500 s before the surface was fully covered by additional liposomes. The dissipation shift for the DOPC/Tyr-C_{10} liposomes also peaked after nearly 310 s and gradually reduced to plateau at a lower value. This indicates that the supported liposomes became slightly more rigid after adsorbing to the surface; thus, this was interpreted as DOPC/Tyr-C_{10} liposomes crowding the surface and becoming more tightly packed but not rupturing.

Incorporation of 5-mole% HTyr-cupheate into DOPC liposomes resulted in a decrease in the frequency shift for nearly the first 500 s followed by a gradual increase in frequency shift (Fig. 4C, solid line). This is consistent with liposome adhering to the surface and starting to expel some water to deform but remaining unruptured. The dissipation shift reached two plateaus (Fig. 4D, solid line), the first of which was achieved nearly 350 s after introducing liposomes across the silica sensor; the second one began after nearly 815 s, stabilizing at ~1525 s before starting a slight downward trend after ~3245 s, indicating that liposomes "soften" minutes after adsorbing. Tyr-cupheate incorporated into DOPC liposomes at 5-mole% resulted in a larger frequency shift that maximized after ~587 s (Fig. 4C, dotted line) which was a slightly longer adsorption process than that for HTyr-cupheate liposomes. This was interpreted as more Tyr-cupheate liposomes adsorbing onto the silica than HTyr-cupheate liposomes since both HTyr- and Tyr-cupheate liposomes were statistically the same size (116 ± 4 nm and 118 ± 4 nm, respectively). The frequency shift for Tyr-cupheate liposomes also increases after 1000 s, indicating that liposomes expelled some water to deform. The dissipation shift (Fig. 4D, dotted line) had a single plateau with some undulation which further suggests that liposomes deformed.

More detailed information about structural changes of adsorbed material was discernible by plotting ΔD vs. ΔF which removes time explicitly [34,35]. Shown in Fig. 4E are the pathways of adsorption for all liposomes studied with the different HTyr and Tyr derivatives incorporated. Liposomes consisting of only DOPC (dark red line) displayed the typical "cusp" shape during liposome adsorption on silica where liposomes adsorbed to a maximum, rapidly fused (ΔD increased to a maximum value simultaneously as ΔF decreased to a minimum) and ruptured (ΔD reduced to a minimum as ΔF simultaneously increased to a maximum value) to form a supported bilayer (Scheme 1a) [32]. DOPC/HTyr-C_{10} liposomes (dashed orange line) exhibited the same "cusp" behavior but to a higher ΔD maximum and larger negative ΔF value which indicates that more mass (liposomes) were adsorbed before fusion and rupture occurred for DOPC/HTyr-C_{10} liposomes. The final result was that DOPC/HTyr-C_{10} liposomes structurally formed a similar supported bilayer as DOPC liposomes (evident by practically the same final ΔF; Scheme 1a).

The other derivatives (Tyr-C_{10}, HTyr-cupheate, and Tyr-cupheate) had markedly different effects on DOPC liposome structural rearrangements. Liposomes containing these individual derivatives exhibited nearly linear ΔD–ΔF plots (increasing ΔD, decreasing ΔF) for the bulk of the adsorption process, which is the typical sign of single-stage adsorption of intact liposomes onto a surface [32]. However, significantly different structural rearrangements occurred for each. For instance, the ΔD–ΔF plot for DOPC/Tyr-C_{10} (dashed yellow line) remained linear to a ΔD maximum of nearly 14 and a ΔF minimum nearly −100 Hz before a small "cusp" formed. Indications here were that significantly more DOPC/Tyr-C_{10} liposomes adsorbed than DOPC or DOPC/HTyr-C_{10} liposomes before rapid fusion onset. The "cusp" for DOPC/Tyr-C_{10} liposomes then proceeded downward slightly, indicating that some liposomes ruptured to form a supported bilayer. Finally, the "cusp" exhibited a gradual decrease in ΔD to a value of 11 with a gradual decrease of ΔF to ~−129 Hz, suggesting that more liposomes deposited, deformed (mass loss from some expelled aqueous contents), and formed a rigid supported liposomal layer (Scheme 1b).

DOPC/HTyr-cupheate liposomes exhibited a nearly linear ΔD–ΔF plot until a frequency shift of ~−60 Hz (dashed green line) and a dissipation shift of ~9 before it started to curve downward slightly ending near −120 Hz and leveling at a ΔD value about 12. This was interpreted as liposomes starting to slowly fuse without rupturing as more liposomes continued to deposit. The ΔD–ΔF plot then reversed abruptly in ΔF, increasing while maintaining the ΔD value of 12. There was then a sudden vertical increase of ΔD to about 16 with a moderate increase in ΔF only to have ΔD finally leveled at nearly 17 while ΔF decreased to ~−90 Hz. It was interpreted as a small number of liposomes adsorbed and instantaneously expelled water to form a supported bilayer. This in turn triggered some liposomal rearrangement (possibly adsorption of deformed liposomes or local swelling) resulting in a "softer" supported liposome film where one or two liposomes began to release their contents at a time (Scheme 1c).

DOPC/Tyr-cupheate liposomes (blue dotted line) displayed a similar trend as DOPC/HTyr-cupheate liposomes with the following differences: 1) the plot appeared to maintain linearity longer, up to approximate ΔD and ΔF values of 11 and −95 Hz, respectively, before starting a downward curve ending near ΔD and ΔF values of 12 and −140 Hz, respectively; 2) the plot then circles back, increasing in ΔF from ~−140 Hz to ~−130 Hz while having small fluctuations in ΔD near 11; and 3) finally, there was an abrupt increase in ΔD from ~11 to 14. The interpretation here was DOPC/Tyr-cupheate required more liposomes to deposit than DOPC/HTyr-cupheate before fusion started. Liposome fusion then triggered rupture which itself triggered liposomal rearrangement without further release of contents (similar to Scheme 1c with subtle differences).

Finally, analysis of the initial slope of the ΔD–ΔF plots gave an indication of the strength of the liposome–surface interactions at the beginning of adsorption where the more shallow the slope equates to stronger liposome–surface interactions [32,36]. The insert in Fig. 4E shows that liposome–surface interactions follow the order DOPC/Tyr-cupheate > DOPC ≈ DOPC/HTyr-C_{10} ≈ DOPC/Tyr-C_{10} > DOPC/HTyr-cupheate, suggesting that liposome–surface interactions on silica were more important in adsorption for the Tyr-cupheate liposomes than the others.

Surprisingly, there was such markedly different adsorption, fusion and rupture behavior of the DOPC liposomes doped with Tyr and HTyr derivatives synthesized from decanoic acid and cuphea oil, especially since derivatives from either decanoic acid and cuphea oil are structurally the same (Fig. 5). A partial explanation may lie in the fact that HTyr

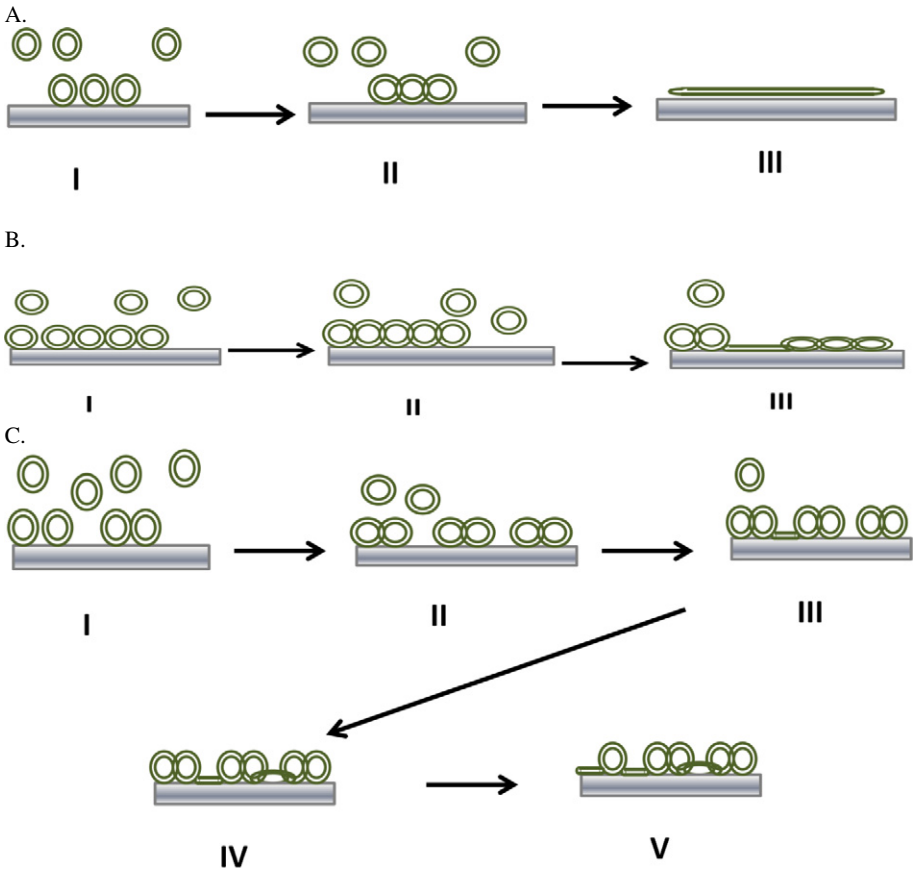

Scheme 1. Illustration of the adsorption process onto silica for liposomes containing (A) DOPC and HTyr-C_{10}, (B) Tyr-C_{10}, and (C) HTyr-cupheate or Tyr-cupheate.

and Tyr have two slightly different predicted pKa values (unpublished data) which may alter liposomal surface charge [37]. Presumably, the different pKa values will induce different surface charges on the liposomes which can make the difference in adsorption behavior as demonstrated with liposomes doped with varying concentrations of an anionic phospholipid [29,38]. There may be concern for lipid impurities remaining in the stock derivatives from unreacted decanoic acid, or unreacted $C_{8:0}$–$C_{18:3}$ fatty acids and di-/triacylglycerides from cuphea oil. Previously C_{10}–C_{23} hydrocarbons were shown to enhance fusion of phosphatidylcholine liposomes by reducing the free energy barrier of the hydrophobic interstices [39–41]. Therefore, it is reasonable to expect that such effects in DOPC liposomes adsorbing onto a surface would induce an enhanced rate of rupture and result in faster rupture. This, however, was not the case in each system studied. Liposome fusion on silica, instead, was slowed or limited which suggests that phenyl hydroxyl groups exerted the greater influence in DOPC/HTyr-C_{10} and DOPC/Tyr-C_{10} adsorption behavior than any impurities from $C_{8:0}$–$C_{18:3}$ fatty acids. Di- and triacylglycerides, alternatively, can conceivably delay liposomal fusion because they can reside within the interstitial region of a bilayer and increase bilayer width [42] which in turn could raise the activation energy for rupture. This could explain, at least partially, the similar slower fusion process for the cupheate liposomes. However, this does not necessarily explain the loss of aqueous contents at the end of the adsorption process displayed by DOPC/HTyr-cupheate liposomes or the loss of contents seen for DOPC/Tyr-cupheate liposomes. It is probable that the HTyr and Tyr moieties were contributing to these behaviors, similarly to DOPC/HTyr-C_{10} liposomes that exhibited greater loss of aqueous contents than DOPC/Tyr-C_{10} liposomes.

In conclusion, this work demonstrates that HTyr and Tyr esters enzymatically synthesized from cuphea oil and decanoic acid partitioned and resided at the aqueous interface of phospholipid liposomes. Partitioning was shown to be similar for both Tyr derivatives and both HTyr derivatives, where HTyr derivatives partition slightly more their Tyr counterparts. It was also demonstrated that there was a marked difference in bilayer behavior on a silica surface due to the Tyr and HTyr moieties where HTyr led to more liposomes rupturing on the surface. Both Tyr and HTyr derivatives have demonstrated the ability to reduce or prevent liposome rupture on silica. The limited liposome rupture on silica was presumably due to reduced membrane tension which is a major contributing component to liposome fusion and rupture on a surface [25], demonstrating the ability of the Tyr and HTyr esters to increase the stability of liposomes. Increased stability of liposomes equates to longer durability, longer shelf-life and longer circulation.

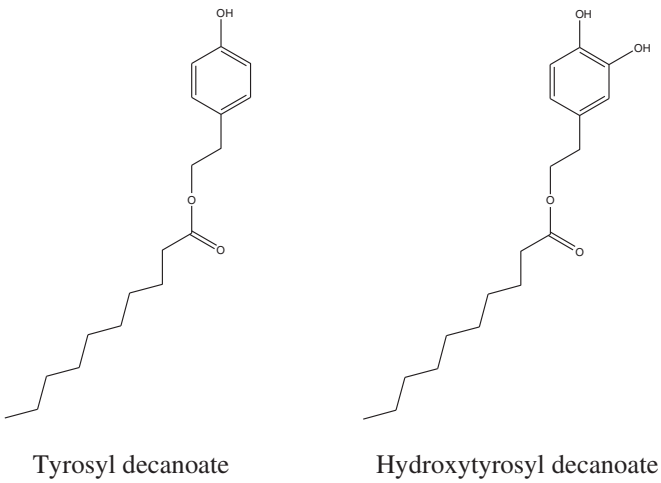

Fig. 5. Structures of tyrosyl and hydroxytyrosyl decanoates synthesized from cuphea oil or decanoic acid.

Considering the fact that Tyr and HTyr esters synthesized from cuphea oil increased liposomal stability and demonstrated the potential to improve the oxidative stability of sensitive fatty acids in food applications further indicates that liposomes loaded with the cupheates can be utilized in food industry.

Transparency document

The Transparency document associated with this article can be found, in the online version.

Acknowledgment

The authors are grateful for the technical assistance provided by Leslie Smith and Nathan Whitman.

References

[1] D. Berti, G. Caminati, P. Baglioni, Functional liposomes and supported lipid bilayers: towards the complexity of biological archetypes, Phys. Chem. Chem. Phys. 13 (2011) 8769–8782.
[2] C. Tan, S. Xia, J. Xue, J. Xie, B. Feng, X. Zhang, Liposomes as vehicles for lutein: preparation, stability, liposomal membrane dynamics, and structure, J. Agric. Food Chem. 61 (2013) 8175–8184.
[3] D.J. McClements, Design of nano-laminated coatings to control bioavailability of lipophilic food components, J. Food Sci. 75 (2010) R30–R42.
[4] G. Caramia, A. Gori, E. Valli, L. Cerretani, Virgin olive oil in preventive medicine: from legend to epigenetics, Eur. J. Lipid Sci. Technol. 114 (2012) 375–388.
[5] F. Visioli, Olive oil phenolics: where do we stand? Where should we go? J. Sci. Food Agric. 92 (2012) 2017–2019.
[6] R. Mateos, M. Trujillo, G. Pereira-Caro, A.s. Madrona, A. Cert, J.L. Espartero, New lipophilic tyrosyl esters. Comparative antioxidant evaluation with hydroxytyrosyl esters, J. Agric. Food Chem. 56 (2008) 10960–10966.
[7] F. Shahidi, Y. Zhong, Revisiting the polar paradox theory: a critical overview, J. Agric. Food Chem. 59 (2011) 3499–3504.
[8] M.l. Laguerre, L.J. López Giraldo, J.r.m. Lecomte, M.-C. Figueroa-Espinoza, B. Baréa, J. Weiss, E.A. Decker, P. Villeneuve, Relationship between hydrophobicity and antioxidant ability of "phenolipids" in emulsion: a parabolic effect of the chain length of rosmarinate esters, J. Agric. Food Chem. 58 (2010) 2869–2876.
[9] M.l. Laguerre, L.J. López Giraldo, J.r.m. Lecomte, M.-C. Figueroa-Espinoza, B. Baréa, J. Weiss, E.A. Decker, P. Villeneuve, Chain length affects antioxidant properties of chlorogenate esters in emulsion: the cutoff theory behind the polar paradox, J. Agric. Food Chem. 57 (2009) 11335–11342.
[10] D. Tofani, V. Balducci, T. Gasperi, S. Incerpi, A. Gambacorta, Fatty acid hydroxytyrosyl esters: structure/antioxidant activity relationship by ABTS and in cell-culture DCF assays, J. Agric. Food Chem. 58 (2010) 5292–5299.
[11] R. Lucas, F. Comelles, D. Alcántara, O.S. Maldonado, M. Curcuroze, J.L. Parra, J.C. Morales, Surface-active properties of lipophilic antioxidants tyrosol and hydroxytyrosol fatty acid esters: a potential explanation for the nonlinear hypothesis of the antioxidant activity in oil-in-water emulsions, J. Agric. Food Chem. 58 (2010) 8021–8026.
[12] J.A. Laszlo, S.C. Cermak, K.O. Evans, D.L. Compton, R. Evangelista, M.A. Berhow, Medium-chain alkyl esters of tyrosol and hydroxytyrosol antioxidants by cuphea oil transesterification, Eur. J. Lipid Sci. Technol. 115 (2013) 363–371.
[13] P. Košinová, K. Berka, M. Wykes, M. Otyepka, P. Trouillas, Positioning of antioxidant quercetin and its metabolites in lipid bilayer membranes: implication for their lipid-peroxidation inhibition, J. Phys. Chem. B 116 (2011) 1309–1318.
[14] O. Fadel, K. El Kirat, S. Morandat, The natural antioxidant rosmarinic acid spontaneously penetrates membranes to inhibit lipid peroxidation in situ, Biochim. Biophys. Acta 1808 (2011) 2973–2980.
[15] G. Knothe, S.C. Cermak, R.L. Evangelista, Cuphea oil as source of biodiesel with improved fuel properties caused by high content of methyl decanoate†, Energy Fuel 23 (2009) 1743–1747.
[16] A. Kyrychenko, F. Wu, R.P. Thummel, J. Waluk, A.S. Ladokhin, Partitioning and localization of environment-sensitive 2-(2′-pyridyl)- and 2-(2′-pyrimidyl)-indoles in lipid membranes: a joint refinement using fluorescence measurements and molecular dynamics simulations, J. Phys. Chem. B 114 (2010) 13574–13584.
[17] A. Chattopadhyay, E. London, Parallax method for direct measurement of membrane penetration depth utilizing fluorescence quenching by spin-labeled phospholipids, Biochemistry 26 (1987) 39–45.
[18] M. Kondo, M. Mehiri, S.L. Regen, Viewing membrane-bound molecular umbrellas by parallax analyses, J. Am. Chem. Soc. 130 (2008) 13771–13777.
[19] B.A. Lewis, D.M. Engelman, Lipid bilayer thickness varies linearly with acyl chain length in fluid phosphatidylcholine vesicles, J. Mol. Biol. 166 (1983) 211–217.
[20] K. Kachel, E. Asuncion-Punzalan, E. London, The location of fluorescence probes with charged groups in model membranes, Biochim. Biophys. Acta 1374 (1998) 63–76.
[21] F. Höök, B. Kasemo, T. Nylander, C. Fant, K. Sott, H. Elwing, Variations in coupled water, viscoelastic properties, and film thickness of a Mefp-1 protein film during adsorption and cross-linking: a quartz crystal microbalance with dissipation monitoring, ellipsometry, and surface plasmon resonance study, Anal. Chem. 73 (2001) 5796–5804.
[22] R. Cheikhousman, M. Zude, D. Bouveresse, C. Léger, D. Rutledge, I. Birlouez-Aragon, Fluorescence spectroscopy for monitoring deterioration of extra virgin olive oil during heating, Anal. Bioanal. Chem. 382 (2005) 1438–1443.
[23] R. Rezaei-Sadabady, N. Zarghami, A. Barzegar, A. Eidi, A. Akbarzadeh, M. Rezaei-Tavirani, Studies of the relationship between structure and antioxidant activity in interesting systems, including tyrosol, hydroxytyrosol derivatives indicated by quantum chemical calculations, Soft 2 (2013) 13–18.
[24] H. Kitayama, Y. Takechi, N. Tamai, H. Matsuki, C. Yomota, H. Saito, Thermotropic phase behavior of hydrogenated soybean phosphatidylcholine- cholesterol binary liposome membrane, Chem. Pharm. Bull. 62 (2014) 58–63.
[25] W. Shen, J. Hu, X. Hu, Impact of amphiphilic triblock copolymers on stability and permeability of phospholipid/polymer hybrid vesicles, Chem. Phys. Lett. 600 (2014) 56–61.
[26] C. Bonnaud, C.A. Monnier, D. Demurtas, C. Jud, D. Vanhecke, X. Montet, R. Hovius, M. Lattuada, B. Rothen-Rutishauser, A. Petri-Fink, Insertion of nanoparticle clusters into vesicle bilayers, ACS Nano 8 (2014) 3451–3460.
[27] M. Ma, D. Bong, Controlled fusion of synthetic lipid membrane vesicles, Acc. Chem. Res. 46 (2013) 2988–2997.
[28] X. Zhang, S. Yang, Nonspecific adsorption of charged quantum dots on supported zwitterionic lipid bilayers: real-time monitoring by quartz crystal microbalance with dissipation, Langmuir 27 (2011) 2528–2535.
[29] R. Richter, A. Mukhopadhyay, A. Brisson, Pathways of lipid vesicle deposition on solid surfaces: a combined QCM-D and AFM study, Biophys. J. 85 (2003) 3035–3047.
[30] Y. Jing, H. Trefna, M. Persson, B. Kasemo, S. Svedhem, Formation of supported lipid bilayers on silica: relation to lipid phase transition temperature and liposome size, Soft Matter 10 (2014) 187–195.
[31] E. Reimhult, F. Höök, B. Kasemo, Vesicle adsorption on SiO_2 and TiO_2: dependence on vesicle size, J. Chem. Phys. 117 (2002) 7401–7404.
[32] E. Reimhult, F. Höök, B. Kasemo, Intact vesicle adsorption and supported biomembrane formation from vesicles in solution: influence of surface chemistry, vesicle size, temperature, and osmotic pressure, Langmuir 19 (2003) 1681–1691.
[33] B. Seantier, C. Breffa, O. Felix, G. Decher, In situ investigations of the formation of mixed supported lipid bilayers close to the phase transition temperature, Nano Lett. 4 (2004) 5–10.
[34] F. Höök, M. Rodahl, P. Brzezinski, B. Kasemo, Energy dissipation kinetics for protein and antibody-antigen adsorption under shear oscillation on a quartz crystal microbalance, Langmuir 14 (1998) 729–734.
[35] Z. Wang, S. Yang, Adsorption behaviors of DPPC/MO aggregates on SiO_2 surfaces, Langmuir 24 (2008) 11616–11624.
[36] M. Sundh, S. Svedhem, D.S. Sutherland, Formation of supported lipid bilayers at surfaces with controlled curvatures: influence of lipid charge, J. Phys. Chem. B 115 (2011) 7838–7848.
[37] V. Pector, J. Caspers, S. Banerjee, L. Deriemaeker, R. Fuks, A. El Ouahabi, M. Vandenbranden, R. Finsy, J.-M. Ruysschaert, Physico-chemical characterization of a double long-chain cationic amphiphile (Vectamidine) by microelectrophoresis, Biochim. Biophys. Acta 1372 (1998) 339–346.
[38] R.P. Richter, A.R. Brisson, Following the formation of supported lipid bilayers on mica—a study combining AFM, QCM-D and ellipsometry, Biophys. J. 88 (2005) 3422–3433.
[39] G. Basáñez, F.M. Goñi, A. Alonso, Effect of single chain lipids on phospholipase C-promoted vesicle fusion. A test for the stalk hypothesis of membrane fusion†, Biochemistry 37 (1998) 3901–3908.
[40] Z. Chen, R.P. Rand, Comparative study of the effects of several n-alkanes on phospholipid hexagonal phases, Biophys. J. 74 (1998) 944–952.
[41] V.S. Malinin, P. Frederik, B.R. Lentz, Osmotic and curvature stress affect PEG-induced fusion of lipid vesicles but not mixing of their lipids, Biophys. J. 82 (2002) 2090–2100.
[42] R. Li, W. Schmidt, S. Rankin, R.L. Walzem, E. Boyle-Roden, Solubilization of acyl heterogeneous triacylglycerol in phosphatidylcholine vesicles, J. Agric. Food Chem. 51 (2003) 477–482.